# Empirical-Stochastic LMS-MIMO Channel Model Implementation and Validation

Peter R. King, Tim W.C. Brown, *Member, IEEE*, Argyrios Kyrgiazos
and Barry G. Evans, *Senior Member, IEEE*

***Abstract*—Land Mobile Satellite (LMS) networks, forming a key component of future mobile Internet and broadcasting, can benefit from Multiple-Input Multiple-Output (MIMO) techniques to improve spectral efficiency and outage. LMS-MIMO networks can be obtained using multiple satellites with single polarization antennas with spatial multiplex channel coding, or by a single satellite with dual polarization antennas providing polarization multiplex channel coding. In this paper, a guide is presented showing the steps required to implement a simple empirical-stochastic dual circular polarized LMS-MIMO narrowband channel model with validation both with and without a line of sight. The model is based on an S-band tree-lined road measurement campaign using dual circular polarizations at low elevations. Application of the model is aimed at LMS-MIMO physical layer researchers and system designers, who need an easy to implement and reliable model, representative of typical LMS-MIMO channel conditions.**

***Index Terms*—LMS (Land Mobile Satellite), MIMO (Multiple-Input Multiple-Output), Channel Model, Stochastic, Propagation**

## I. Introduction

The benefit of applying MIMO (Multiple-Input Multiple-Output) techniques to the LMS (Land Mobile Satellite) channel, in terms of capacity gain and diversity gain, was shown in [1] and [2] respectively. In recent years, the use of MIMO in terrestrial wireless systems including the next generation wireless networks, IEEE 802.11n [3] as well as wide area networks, IEEE 802.16m [4] and long term evolution of third generation mobile (3GPP LTE) [5] has become widespread. More recently the use of MIMO for LMS has gained interest with regards to satellite based digital video broadcasting standards DVB-SH and DVB-NGH [6]. However, before LMS-MIMO systems are in widespread use, suitable and simple to implement channel models that give a general model of the radio environment are required. This paper defines an empirical-stochastic channel model for such use.

As is typical for LMS channel models, as well as the model presented in this paper, large scale fading comprises Markov Chains to represent the 'on/off' nature of the channel and filtered log-normal simulation to represent the shadowing effects, and Ricean simulation to represent the small scale fading effects [7]. However, this model extends the capabilities to the MIMO case, where its stochastic properties are derived from an S-band tree-lined road measurement campaign using dual circular polarizations at low elevations. Furthermore, this model in particular compared to existing models to date [8][9] considers the interdependence between the small scale fading. The authors have found the most appropriate means to accommodate this interdependence is to use a Ricean fading model, where the co-polar and cross-polar components are suitably correlated.

Section two of this paper describes the typical factors unique to a dual circular polarization LMS-MIMO channel modeling, including the need for a four-state Markov chain to form simultaneous dual polar shadowing models as well as small-scale fading models. This is followed by sections detailing the measurement campaign carried out to show the Markov chain behavior in the LMS-MIMO channel. A step by step guide is then provided in generating the proposed empirical-stochastic model informed by measurement data. The reader can use the information presented to implement the necessary code for such a model. Finally validation tests are shown to clarify the model's application in both line of sight and non line of sight regions.

## II. LMS-MIMO Channel Model Construction

The structure of an LMS-MIMO channel model is a 2x2 MIMO system whereby the two antennas at each end are dual circular polarized with right hand and left hand circular polarizations (RHCP and LHCP) as illustrated in Figure 1.

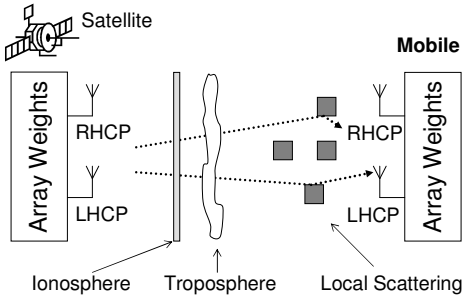


**Figure 1 - Diagram of satellite MIMO channel structure**

The model presented in this paper is considered to be suitable for the L-band and S-band frequency ranges such that the ionospheric and tropospheric effects are considered negligible. The largest impact would be Faraday rotation in the

Manuscript received June 30, 2009. This work was supported in part by the EU FP6 project SatNex (Satellite Communications Network of Excellence).

P. R. King, T. W. C. Brown, A. Kyrgiazos and B. G. Evans are with the Centre for Communication Systems Research at the University of Surrey, U.K. (e-mail: {p.king | t.brown | a.kyrgiazos | b.evans}@surrey.ac.uk).

ionosphere [7], which would be overcome using circular polarization. Ignoring any ionospheric and tropospheric effects, the main item of interest for satellite MIMO is the multipath caused by local scatterers near to the mobile. The scattering caused in this region will create some depolarization from RHCP to LHCP and from LHCP to RHCP, which are represented in a 2x2 MIMO channel matrix, **H**, where there are two co-polar (RHCP to RHCP and LCHP to LHCP) and two cross-polar circularly polarized channels (RHCP to LHCP and LCHP to RHCP). These four channels are conveniently represented as follows with subscripts R and L:

$$\mathbf{H} = \begin{pmatrix} h_{\mathrm{RR}} & h_{\mathrm{LR}} \\ h_{\mathrm{RL}} & h_{\mathrm{LR}} \end{pmatrix} \tag{1}$$

where the channel matrix is used as the multiplicative component within the channel so that the output signal vector received at the mobile, $\mathbf{y}(t)$ relates to the input signal vector $\mathbf{x}(t)$ by the following equation:

$$\mathbf{y}(t) = \mathbf{H}(t)\mathbf{x}(t) + \mathbf{n}(t) \tag{2}$$

where $\mathbf{n}(t)$ is a vector to represent additive white Gaussian noise at the receiver. It is therefore of interest to model the channel state at time $t$, $\mathbf{H}(t)$. The simplest means to model the LMS-MIMO channel is to use a stochastic random process, which will define the distribution of channel states (or first order statistics), but it is also necessary to define how the channel evolves, by considering what is known as the second order statistics.

For satellite MIMO, it is best to break the channel **H** into three components:

1. **Free space path loss** – This is defined theoretically by the well known Friis' formula [7] though for convenience of being able to analyze the channel, it is normalized in this case, since it is merely an offset value.
2. **Shadowing or large scale fading** – When the mobile is on the ground, it may either have a direct line of sight link to the satellite, or there may be a building, tree or other large scattering object blocking the direct path. Thus the mobile is within the shadow of the scatterer and will be subject to extra path loss. In the case of satellite communications, the mobile is constantly moving in and out of the shadow regions as illustrated in Figure 2. Here the mobile is a vehicle moving along the road, it will enter regions between scatterers on its left hand side where it will have a line of sight link with the satellite. Therefore there is a need to statistically model scenarios where there is both high and low shadowing. Therefore it is necessary to model when the mobile is switching between high and low shadowing, which is best achieved by using a Markov chain [10].
3. **Small scale fading** – In the local area around the mobile there will be several scattering objects, which will produce reflected, refracted and diffracted signals. As the mobile moves, these reflections, refractions and diffractions are constantly changing and thus the received signal is constantly changing. In some instances, the reflected signals will add up constructively in phase, while in other cases they will add up destructively out of phase and the received signal will go into a deep fade.

It is therefore necessary to separately model the small scale and large scale fading characteristics of the channel $\mathbf{H}(t)$ as it changes over time with mobile movement.

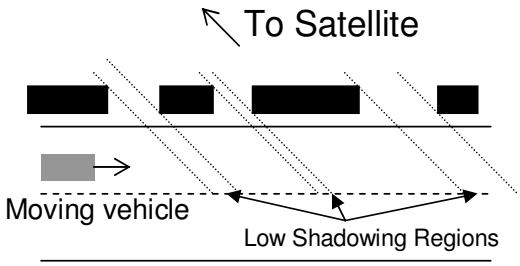


**Figure 2 - Diagram illustrating an example of high and low shadowing regions**

For LMS-MIMO, there are a number of modeling challenges not addressed in other LMS channel models that must be considered and which have led to the construction of a simple to implement stochastic model provided in this paper. The factors that require consideration include the following:

- The MIMO branches are in the circular polarization domain, rather than the spatial domain. Therefore, channel multiplexing occurs in this domain, which will give different characteristics in the eigen decomposition of the channel, as will be seen from measurement data later in this paper. Therefore different eigen characteristics [11] from conventional MIMO channel models need to be modeled.
- The large scale fading changes constantly when switching from high to low shadowing. This produces different characteristics for the co-polar and cross-polar channel branches and likewise should be modeled to be consistent with simultaneous measurements of these channels. Furthermore the shadowing characteristics should be compared for both polarizations so that their interdependence is maintained.
- The small scale fading channels for each of the four MIMO paths are not necessarily independent, especially when there is a line of sight link. Therefore in such circumstances, the interdependence must be appropriately modeled so that both the model and real measured data have comparable eigen decomposition.

Before developing models, the Markov chain, polarization and interdependence characteristics need to be identified from real measurement data, which the next section of this paper addresses. After describing the measurements, this paper

describes the stages involved in creating the large scale fading characteristics, Markov chain and small scale fading.

## III. Measurement Setup

Extensive measurements were carried out on the edge of the town of Guildford, UK, representative of a suburban/rural area that would be applicable to LMS-MIMO during the summer time (with trees in full foliage). An artificial terrestrially based platform (acting as a satellite) was placed on top of a hill overlooking a road, as illustrated in Figure 3 containing directional RHCP and LHCP antennas, spaced just under one wavelength apart. Each antenna had a gain of 12dBi and a 3dB beamwidth of 30°. A mobile van contained the receiver and its roof was fitted with an omnidirectional RHCP and LHCP antenna spaced four wavelengths apart. These two antennas had a beamwidth of 70° in elevation. The satellite elevation angles ranged from 7° to 18° as the mobile moved along the tree-lined road. Although many operational satellite elevations exceed these, some geostationary and low Earth orbiting mobile satellite services are required to work at low elevations. The present experiment therefore represents these as worst case system scenarios, where such elevations enable the highest degrees of multipath. Varying levels of Rice factor, as defined by the Ricean distribution, as well as channel correlations provide a usefully wide range of empirical results.

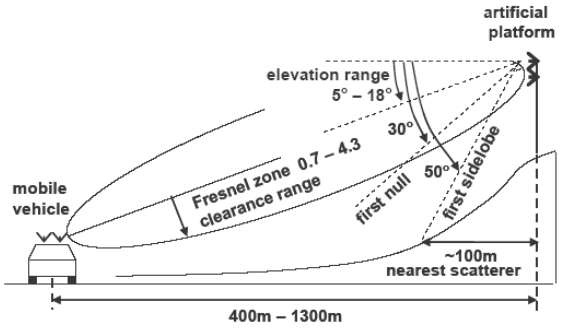


**Figure 3 - Diagram of measurement setup of artificial platform**

An Elektrobit Propsound wideband MIMO channel sounder was configured for a carrier frequency of 2.45GHz and a bandwidth of 200MHz. Each MIMO channel was obtained sequentially by using fast switching at a rate of 152.7Hz, which is over twice the maximum Doppler shift of 73Hz for the vehicle speed, thus meeting Nyquist criteria. This is assumed to be the case on the tree-lined road where there were few vehicles in motion.

Within the data, suitable results were found whereby the channel could be captured within the channel sounder's sensitivity giving a signal to noise ratio that enabled the multipath to be measured without error due to receiver noise. There were many cases of interference from local wireless area networks that had to be filtered out from the measurement data and replaced with interpolated data. Data sampling being more than the required Nyquist criteria meant it was possible to achieve this.

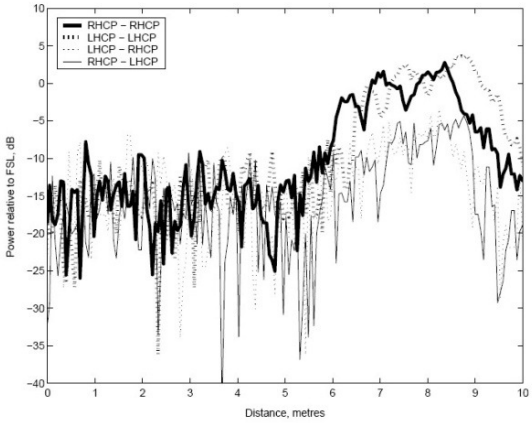


**Figure 4 - Sample measurement showing the Markov chain characteristics of the LMS-MIMO channel**

An example of the measurement data obtained to illustrate the Markov chain behavior of the high and low shadowing is shown in Figure 4 for all four MIMO branches. For clarity, the free space loss (FSL) is normalized out of the channel. Clearly it can be seen that there are different small scale fading characteristics in high and low shadowing regions, as well as Markov chain characteristics that are related for co-polar and cross-polar channels though they are required to be generated separately. The next section will explain in detail how the large scale fading, Markov chain and small scale fading are generated in three separate steps and then integrated in order to form a working channel matrix.

## IV. Model Generation

### *A. Step 1 – Generate large scale fading for high and low shadowing*

For 2x2 MIMO, four simultaneous models of high shadowing that will vary over distance (i.e. in non line of sight region) are required to produce vector $\mathbf{s}_{high}$ and four simultaneous models of low shadowing (i.e. in line of sight region) are required to produce vector $\mathbf{s}_{low}$, in dB by using zero mean, unity standard deviation Gaussian random noise signals.

In order for these two sets of four shadowing models to have interdependence, a 4x4 correlation matrix for large scale fading, $\mathbf{C}_{large}$, is then applied [7] to both high and low shadowing as analysis of measurement data has shown both shadowing cases to follow the necessary Gaussian distribution. This will accommodate the interdependence between the four MIMO branches so that correlated shadowing, $\mathbf{s}_{highlc}$ and $\mathbf{s}_{lowlc}$ is formed as follows:

$$\mathbf{s}_{highlc} = \mathbf{C}_{large}^{½}\mathbf{s}_{high}$$
$$\mathbf{s}_{lowlc} = \mathbf{C}_{large}^{½}\mathbf{s}_{low} \quad (3)$$

where the ½ denotes the Cholesky factorization. An appropriate set of values for $\mathbf{C}_{large}$ are taken from the measurement data representing a typical tree lined road in a suburban environment. To assist with understanding the

matrix formation, the matrix has notations for each element where as an example, the correlation, $c_{\text{large|RR,LL}}$ gives the correlation of the shadowing between the right to right hand branch and the left to left hand branch. Therefore all sixteen possible permutations of this notation are shown in the matrix as follows, from which values from the measured data are then given:

$$\mathbf{C}_{\text{large}} = \begin{pmatrix} c_{\text{large|RR,RR}} & c_{\text{large|LL,RR}} & c_{\text{large|RL,RR}} & c_{\text{large|LR,RR}} \\ c_{\text{large|RR,LL}} & c_{\text{large|LL,LL}} & c_{\text{large|RL,LL}} & c_{\text{large|LR,LL}} \\ c_{\text{large|RR,RL}} & c_{\text{large|LL,RL}} & c_{\text{large|RL,RL}} & c_{\text{large|LR,RL}} \\ c_{\text{large|RR,LR}} & c_{\text{large|LL,LR}} & c_{\text{large|RL,LR}} & c_{\text{large|LR,LR}} \end{pmatrix}$$

$$\mathbf{C}_{\text{large}} = \begin{pmatrix} 1 & 0.86 & 0.85 & 0.9 \\ 0.86 & 1 & 0.91 & 0.9 \\ 0.85 & 0.91 & 1 & 0.88 \\ 0.9 & 0.87 & 0.88 & 1 \end{pmatrix} \quad (4)$$

The correlation values are high, as expected due to the close proximity of the two transmit and two receive antennas and other measurements have shown that high correlation is maintained in different channel scenarios. Using these correlations, eight time-synchronized simulations are created that are defined by the following process in order to form the second order statistics [12][13]:

$$\mathbf{s}_{\text{high|cf}}(n) = \mathbf{s}_{\text{high|c}}(n) + e^{-\frac{v_m \Delta t}{r_c}} \mathbf{s}_{\text{high|cf}}(n-1)$$
$$\mathbf{s}_{\text{low|cf}}(n) = \mathbf{s}_{\text{low|c}}(n) + e^{-\frac{v_m \Delta t}{r_c}} \mathbf{s}_{\text{low|cf}}(n-1) \quad (5)$$

where the time variation is determined by a coherence distance, $r_c$ for a given mobile speed, $v_m$ with sample time $\Delta t$ and $\mathbf{s}_{\text{high}|c}$ and $\mathbf{s}_{\text{low}|c}$ are the correlated Gaussian distributed random variables with zero mean and unity standard deviation. Measurements used in this paper have shown $r_c$ to be 25m on average for a tree-lined road environment. The range of $r_c$ values recorded spanned from 23m through to 29m. It is assumed in this case that each sample, $n$, is taken for every meter. The shadowing then requires normalization where a set of standard deviations to the shadowing represented by vectors $\boldsymbol{\sigma}_{\text{high}}$ and $\boldsymbol{\sigma}_{\text{low}}$ and mean values, represented by vectors $\boldsymbol{\mu}_{\text{high}}$ and $\boldsymbol{\mu}_{\text{low}}$, all in dB, are applied, where ° denotes elementwise multiplication and the normalized, filtered and correlated shadowing, $\mathbf{s}_{\text{high|cfn}}$ and $\mathbf{s}_{\text{low|cfn}}$ are therefore:

$$\mathbf{s}_{\text{high|cfn}} = \left( \mathbf{s}_{\text{high|cf}} \circ \boldsymbol{\sigma}_{\text{high}} \circ \sqrt{1 - e^{-\frac{2 v_m \Delta t}{r_c}}} \right) + \boldsymbol{\mu}_{\text{high}}$$
$$\mathbf{s}_{\text{low|cfn}} = \left( \mathbf{s}_{\text{low|cf}} \circ \boldsymbol{\sigma}_{\text{low}} \circ \sqrt{1 - e^{-\frac{2 v_m \Delta t}{r_c}}} \right) + \boldsymbol{\mu}_{\text{low}} \quad (6)$$

Empirical values of standard deviations $\boldsymbol{\sigma}_{\text{high}}$ and $\boldsymbol{\sigma}_{\text{low}}$ and mean values, $\boldsymbol{\mu}_{\text{high}}$ and $\boldsymbol{\mu}_{\text{low}}$ for co-polar and cross-polar channels in the tree-lined road environment in dB are shown in Table 1, which are derived generically from all measurement data taken as the highest and lowest values. Finally the data must be reshaped to create two separate 2x2 channel matrices $\mathbf{H}_{\text{high}}$ and $\mathbf{H}_{\text{low}}$.

| Polarization | High shadowing (dB) | | Low shadowing (dB) | |
|---|---|---|---|---|
| | $\boldsymbol{\mu}_{\text{high}}$ | $\boldsymbol{\sigma}_{\text{high}}$ | $\boldsymbol{\mu}_{\text{low}}$ | $\boldsymbol{\sigma}_{\text{low}}$ |
| Co-polar | -20.5 | 6.5 | -1.5 | 4.0 |
| Cross-polar | -21.5 | 6.0 | -4.5 | 3.0 |

**Table 1 – Shadowing model mean and standard deviations**

### *B. Step 2 - Generate Markov chain*

Having generated data for high and low shadowing sequences, a Markov Chain [10] is used to select between the regions of high and low shadowing for both co-polar and cross-polar channels. This allows the sharp transitions that occur as a mobile moves past buildings as illustrated in Figure 2 to be suitably modeled. Therefore if two polarizations are considered, there are four possible Markov states as illustrated in Figure 5. It is assumed that the behavior is the same whichever of RHCP or LHCP is being transmitted. Once the polarization is defined at the transmit end, these four possible states therefore consider whether the co-polar or cross-polar channels at the receive end are both in a high or low state or in opposite states, as can happen in certain instances. Given that there are four possible states, there are therefore sixteen possible state transitions as shown by the arrows. The Markov chain statistics are extracted from the measurement data (once a threshold is selected for high and low shadowing in the measurement data) and the results are shown in Table 2, which are derived from analyzing the Markov chain of all measurement samples. The Markov chain derived from the measurement data using the chosen threshold was analysed to ensure that where state transitions did occur, they were true cases of a real transitions. There can be cases with extreme low probability where a high state shadowing falls below the threshold while also a low state threshold rises above the threshold. Inspection of the Markov chain removed any of these remotely possible occurrences. The columns of the state transitions represent the probability of one state moving to another listed in the right hand column, while each row represents the probability of moving to the state shown on the right hand column from a previous state shown on the bottom row. Thus the top right hand state transition of 0.1037 is the probability of moving from state “CP High, XP High” to “CP Low, XP Low”, where CP is a co-polar channel and XP is a cross-polar channel. In the majority of cases for this measurement, both CP and XP are in a high shadowing state, which reflects the measurement scenario being a road lined with houses and trees with foliage thus providing dense multipath and the satellite at a low elevation. From applying the Markov chain analysis, sampled every meter, to the large scale shadowing, a 2x2 channel matrix, $\mathbf{H}_{\text{large}}$ can finally be created.

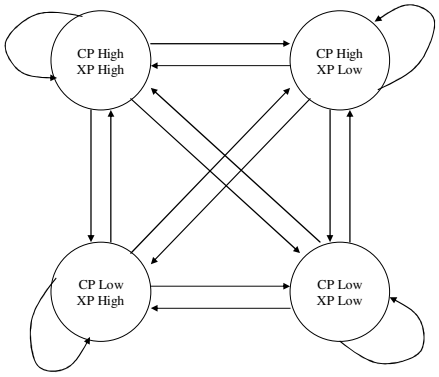


**Figure 5 - Illustration of the four Markov states for the LMS-MIMO channel**

After producing the Markov chain, the data must be up-sampled to match the resolution of the small scale fading that is generated next. Up-sampling is required because the rate of change of fading for the large scale fading is considerably low compared to that of the small scale fading and therefore does not require such a large scale of sampling (based upon the size of $r_c$) in the first instance. However, for the large scale fading to be integrated with the small scale fading at a later stage, it is necessary that the large scale fading matches the necessary sampling rate for the small scale fading.

| State Transitions | | | | State | |
|---|---|---|---|---|---|
| 0.6822 | 0.1579 | 0.0561 | 0.1037 | 0.0764 | CP low XP low |
| 0.2887 | 0.2474 | 0.0447 | 0.4192 | 0.0416 | CP low XP high |
| 0.1682 | 0.0966 | 0.1745 | 0.5607 | 0.0229 | CP high XP low |
| 0.0098 | 0.0199 | 0.0150 | 0.9554 | 0.8591 | CP high XP high |
| CP low XP low | CP low XP high | CP high XP low | CP high XP high | | |

**Table 2 - Markov State and State Transition Table**

*C. Step 3 – Generate small scale fast fading*

The small scale fading is modeled in this case by a Ricean distribution, where the low shadowing region will have a higher Rice factor than that of the high shadowing region, which will be subject to denser multipath. The usage of values of Rice factors based on measurements are discussed later in Table 3.

Using the Rice factors, Ricean fading with appropriate second order statistics can be generated for each MIMO branch by using a ring scatterer model [14] (though other well known methods to generate small scale fading such as Doppler filtering and autocorrelation matrices [7] are equally acceptable). For each sample $n$, the small scale fading elements, denoted by subscripts $_{xx}$ of $\mathbf{H}_{\text{small}}$ are derived in this case as:

$$h_{\text{small}xx}(n) = \frac{\sqrt{k_{xx}}\, e^{j\frac{n2\pi f_m}{N_f}} + \sum_{i=1}^{N_S} M_{\text{norm}} e^{j\left(\frac{2\pi n \sin\phi_i}{N_f} + \theta_i\right)}}{\sqrt{k_{xx}+1}} \tag{7}$$

where $N_f$ is the sampling factor equal to the sampling frequency divided by the maximum Doppler shift, $f_m$ due to mobile movement. The Rayleigh (or scattered) part of the small scale fading is normalized by $M_{\text{norm}}$ so that its mean is unity. The components of the Rayleigh part will arrive at angle $\phi_i$ and have a random phase $\theta_i$. The four $h_{\text{small}xx}$ elements are arranged into the 2x2 matrix $\mathbf{H}_{\text{small}}$.

In the high shadowing regions, there is in general a non line of sight (NLOS) condition and the Rice factor is low. In the case of the LMS, the scatterering rich environment local to the mobile terminal provides low correlation between the antenna branches, while at the satellite there are directional antennas with highly orthogonal circular polarizations, thus their correlation is also low. At each end therefore, the correlation is controlled independently and also remains low in a non line of sight scenario, which therefore justifies that the channel is separable in order to allow the well known Kronecker model to be applied [15] to model the correlated small scale fading, as follows:

$$\text{vec}\left(\mathbf{H}_{\text{small}|c}\right) = \mathbf{R}_{\text{small}|\text{NLOS}}^{1/2}\, \text{vec}\left(\mathbf{H}_{\text{small}|\text{NLOS}}\right) \tag{8}$$

where vec is the vectorize function. Values for the small scale fading correlation matrix are also taken from measurements, where the values are derived as an average of correlation values evaluated over the whole sampled measurement data. The format of matrix $\mathbf{R}_{\text{small}}$ follows the same pattern as that used for $\mathbf{C}_{\text{large}}$ in equation (4):

$$\mathbf{R}_{\text{small}} = \begin{pmatrix} r_{\text{small}\|\text{RR,RR}} & r_{\text{small}\|\text{LL,RR}} & r_{\text{small}\|\text{RL,RR}} & r_{\text{small}\|\text{LR,RR}} \\ r_{\text{small}\|\text{RR,LL}} & r_{\text{small}\|\text{LL,LL}} & r_{\text{small}\|\text{RL,LL}} & r_{\text{small}\|\text{LR,LL}} \\ r_{\text{small}\|\text{RR,RL}} & r_{\text{small}\|\text{LL,RL}} & r_{\text{small}\|\text{RL,RL}} & r_{\text{small}\|\text{LR,RL}} \\ r_{\text{small}\|\text{RR,LR}} & r_{\text{small}\|\text{LL,LR}} & r_{\text{small}\|\text{RL,LR}} & r_{\text{small}\|\text{LR,LR}} \end{pmatrix}$$

$$\mathbf{R}_{\text{small}} = \begin{pmatrix} 1 & 0.03 & 0.02 & 0.09 \\ 0.03 & 1 & 0.12 & 0.01 \\ 0.02 & 0.12 & 1 & 0.01 \\ 0.09 & 0.01 & 0.02 & 1 \end{pmatrix} \tag{9}$$

In the case where there is low shadowing and a line of sight (LOS), the channel cannot be considered separable and thus the Kronecker assumption does not hold. Thus the Kronecker model has been extended here such that it is suited to a 2x2 satellite MIMO system in a LOS environment with dual circular polarization, which enables polarization multiplexing.

Firstly a co-polar correlation matrix, $\mathbf{R}_{\text{CP}}$ (within which a complex correlation [7], $r_{\text{CP}}$ of $h_{\text{RR}}$ and $h_{\text{LL}}$ is used) is defined as the following 2x2 matrix:

$$\mathbf{R}_{CP} = \begin{pmatrix} 1 & r_{CP}^{*} \\ r_{CP} & 1 \end{pmatrix} \quad (10)$$

The phase information in the matrix may be used, though as the validation section later on will clarify, it is not essential to include when generating a model. Secondly a cross polar correlation matrix, $\mathbf{R}_{XP}$ is also defined in a similar way. The correlation component, $r_{XP}$ is derived by taking an average of the complex correlation of $h_{LL}$ and $h_{LR}$ and the correlation of $h_{RR}$ and $h_{RL}$. Again the phase information is not essential and it is assumed the two antennas at the transmit end have similar characteristics in terms of gain patterns and polarization purity. The same must also be true at the receive end, though the transmit antennas do not have to be the same as the receive antennas. The 2x2 correlation matrix for the cross-polar is defined as follows:

$$\mathbf{R}_{XP} = \begin{pmatrix} 1 & r_{XP}^{*} \\ r_{XP} & 1 \end{pmatrix} \quad (11)$$

The two matrices in equations (10) and (11) will influence the orthogonality of the right hand and left hand polarizations, which will be key to a MIMO channel. A 1x2 channel vector of the co-polar components, $\mathbf{h}_{CP|small}$, is then generated using Rice factors determined from measurement using equation (7) and then the two co-polarizations are correlated to gain $\mathbf{h}_{CP|small||C}$ as follows:

$$\mathbf{h}_{CP|small||C} = \mathbf{R}_{CP}^{1/2}\mathbf{h}_{CP|small} \quad (12)$$

Likewise the same can be done for the cross polar components, which have a very different correlation and Rice factor compared to the co-polar case:

$$\mathbf{h}_{XP|small||C} = \mathbf{R}_{XP}^{1/2}\mathbf{h}_{XP|small} \quad (13)$$

The four elements once generated can easily be inserted into a 2x2 matrix to generate the small scale fading, $\mathbf{H}_{small.}$. After applying the correlation, it is necessary to re-normalise the mean values of all four MIMO branches. For the cross polar components, $h_{small|LR}$ and $h_{small|RL}$, the mean values must also be divided by the square root of the cross polar ratio, $\sqrt{XPD}$. The XPD is defined as the ratio of the mean co-polar power to the mean cross-polar power. It is assumed XPD is the same whether the co-polar component is left hand or right hand circularly polarized.

Measurements provided data showing Rice factors ranging from 0 to 10 for co-polar data. The cross polar Rice factors were also found to be wide ranging, though as a rule they are always less than the co-polar Rice factor for a set of samples, thus any Rice factors can be selected for a model that adhere to the rule, though corresponding XPD and correlations have to be used alongside given Rice factors. Table 3 and Table 4 present suitable corresponding values of correlation and XPD respectively taken from analyzing measurement data available.

In the case of a high Rice factor, the co-polar correlation will be inherently high, while for a low Rice factor the correlation is lower and has a greater variance. XPD can be as high as 15dB for a high Rice factor, though on average it is closer to 10dB. For lower Rice factors, where the scattering causes significant de-polarization the average XPD is closer to 0dB.

| **Rice Factor** | **Mean $r_{CP}$** | **$r_{CP}$ Standard Deviation** | **Mean $r_{XP}$** | **$r_{XP}$ Standard Deviation** |
|---|---|---|---|---|
| 0 to 2 | 0.41 | 0.24 | 0.28 | 0.177 |
| 2 to 4 | 0.73 | 0.19 | 0.18 | 0.13 |
| 4 to 10 | 0.87 | 0.0052 | 0.42 | 0.24 |

**Table 3 - Comparison of mean and standard deviation values of complex correlation magnitude against Rice factor**

| **Rice Factor** | **Max XPD (dB)** | **Min XPD (dB)** |
|---|---|---|
| 0 to 2 | 6 | 0 |
| 2 to 4 | 6 | 0 |
| 4 to 10 | 15 | 4 |

**Table 4 - Comparison of maximum and minimum XPD against Rice factor**

### *D. Step 4 – Integrate steps 1, 2 and 3*

Now that the large and small scale fading channels are created, they can simply be multiplied together to form the final channel model such that:

$$\mathbf{H} = \mathbf{H}_{large} \circ \mathbf{H}_{small} \quad (14)$$

where ° denotes an elementwise multiplication of the two matrices. It should be noted that the resultant large scale fading $\mathbf{H}_{large}$ is already normalized to the bulk mean free space path loss and any other losses in the ionosphere or troposphere. However, the resultant small scale fading $\mathbf{H}_{small}$ must be normalised to unity mean power.

## V. LMS-MIMO Channel Model Validation of Small Scale Fading

An important validation for MIMO channel models is to ensure that the eigenvalue cumulative distributions produced by the model are in good agreement with measured data. This will not only ensure that the first and second order statistics of the physical channel are suitably modeled but also that the interdependence between them is suitably accounted for in order to demonstrate the diversity and multiplexing capabilities of the model.

| **Scenario** | XPD (dB) | $k_{CP}$ | $k_{XP}$ | $r_{CP}$ | $r_{XP}$ |
|---|---|---|---|---|---|
| NLOS | 5.9 | 2.43 | 0.97 | 0.65 | 0.34 |
| LOS | 8.1 | 6.01 | 2.04 | 0.92 | 0.61 |

**Table 5 – Correlation, XPD and Rice factor values used in the NLOS and LOS cases for validation**

To demonstrate the validation of the model, two LOS and NLOS cases were chosen, which had values of Rice factor, XPD and correlation shown in Table 5. The values for Rice factor are in linear form.

The following three sub-sections compare the first order, second order and eigen analysis as a validation of the model proposed using appropriate sections of the measurement data. The narrowband measurement data used for validation has a sampling rate of more than twice the maximum Doppler shift so as to meet Nyquist criteria.

### *A. First Order Statistics*

Figure 6 and Figure 7 illustrate the cumulative distribution of the small scale fading for all four branches of the NLOS and LOS regions. In both cases there is good agreement between the measurement data and model, where in the LOS scenario, a wider gap can be identified between co-polar and cross-polar branches. It is interesting to note that the mean value of the cross-polar component for LHCP transmission is shifted by over 6dB when compared to RHCP, where the multipath was found to better combine constructively within the sampled time window. The model, however, has not accommodated this difference, since the negligible contribution of the cross-polar element to the MIMO channel has no real effect on the capacity or eigen analysis.

### *B. Second Order Statistics*

Figure 8 shows the Doppler spread in both left hand to left hand ($h_{\mathrm{LL}}$) and right hand to right hand ($h_{\mathrm{RR}}$) polarized cases, where polarization makes little difference in LOS or NLOS. The Doppler spread shown verifies the suitability of the Ricean distribution for small scale modeling based on a Classical bath tub model with the addition of a delta function for the Rice component [7]. A high Rice component is identified in Figure 8 for the LOS case while still a small Rice component is identified in the NLOS case due to non uniform angle of arrival.

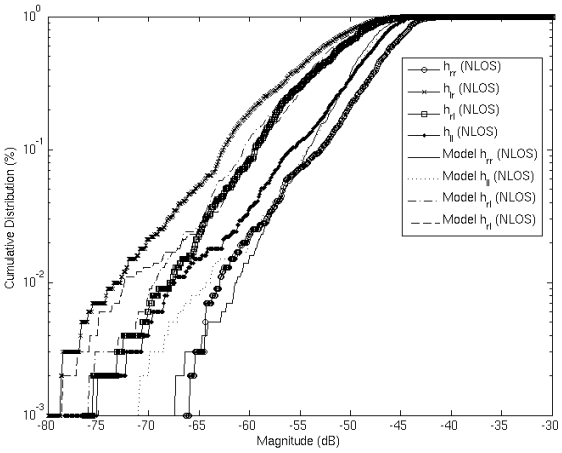


**Figure 6 - Cumulative distribution plot of the modeled and measured channel for high shadowing (NLOS)**

A further validation of the second order statistics is presented in Figure 9, which shows a good agreement between level crossing rate and average fade duration when comparing the measured narrowband data and the modeled narrowband data. Free space loss and the maximum Doppler frequency are labeled FSL and $f_m$ respectively.

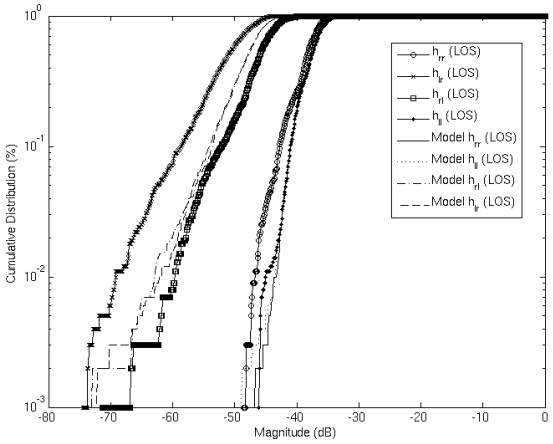


**Figure 7 - Cumulative distribution plot of the modeled and measured channel for low shadowing (LOS)**

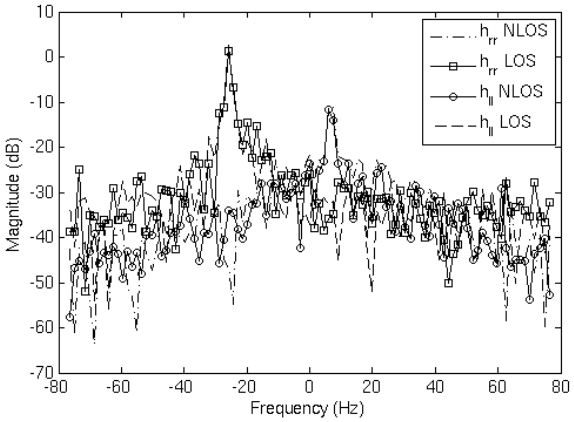


**Figure 8 - Comparison of the right to right hand and left to left hand polarized Doppler spread in NLOS and LOS**

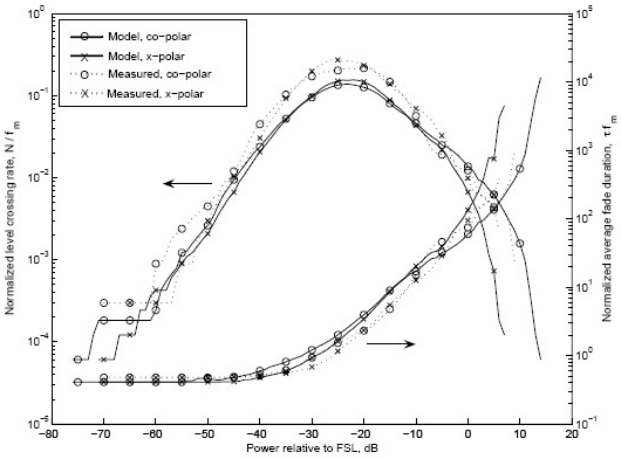


**Figure 9 - Validation of the second order statistics based on level crossing rate and average fade duration**

### C. Eigen-Analysis

Figure 10 presents results of the eigen analysis of the model and measurement data as well as the modeled data for the NLOS case. Clearly there is a good consistency, which verifies the Kronecker model approach is sufficient for this scenario. In this graph, the notation $s_n$ is denoted as an eigenvalue where $n$ is 1 or 2 for a 2x2 MIMO system.

Figure 11 on the other hand compares measured and modeled eigenvalues in the LOS case using the new model approach. Compared to the NLOS case, the LOS channel is clearly rich in polarization multiplexing, as opposed to diversity because the eigenvalue distributions are closer. This is expected due to fewer scatterers. Results are in agreement, though it should be noted that in this validation, the phase information was applied in the correlation matrices. Were the phase information not applied, the second eigenvalue would marginally change its gradient, moving away from the measured data by less than 2dB. Given the negligible impact this would have on modeled channel capacity, use of the phase information is therefore not important. A similar scenario occurs when modeling other LOS regions.

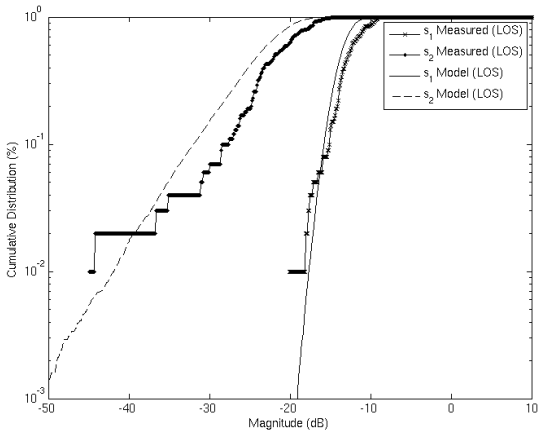


**Figure 10 - Comparison of the model and measurement eigenvalues for the high shadowing (NLOS) region**

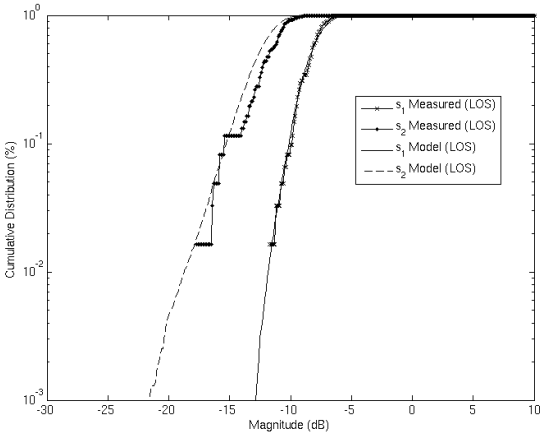


**Figure 11 - Comparison of the model and measurement eigenvalues for the low shadowing (LOS) region**

## VI. Conclusion

The procedure for implementing a simple empirical-stochastic based model for the dual circular polar 2x2 LMS-MIMO channel has been presented along with results to validate the model at low elevation, which is based on switching between high and low shadowing regions with different multipath conditions. The validation of the model at such elevations will also be suited to higher elevation angles where the multipath is reduced and the opportunity to implement polarization multiplexing is increased. The well known Kronecker model is suitable for the non line of sight case, while a new model has been presented to be applied to a polarization multiplexing rich scenario in the line of sight case. Comparisons show good accuracy in both cases. Given the simplicity of generating a Markov chain and correlated small scale and large scale fading, it is highly appropriate for conformance testing for satellite MIMO applications with the simplicity of controlling the channel through altering Rice factors, correlation and XPD values according to guidelines presented.

## Acknowledgment

The help of Mr Unwana Ekpe at the University of Surrey is acknowledged for extracting the relevant narrowband measurement data.

## References

[1] P.R. King, S. Stavrou, “Capacity Improvement for a Land Mobile Single Satellite MIMO System”, IEEE Antennas and Wireless Propagation Letters, vol.5, iss.1, Dec.2006, pp.98-100.

[2] P.R. King, P. Horváth, F. Pérez-Fontán, I. Frigyes, S. Stavrou, “Satellite Channel Impairment Mitigation by Diversity Techniques”, IST Mobile Summit, June 2005.

[3] IEEE 802.11n Standard for Information technology—Telecommunications and information exchange between systems—Local and metropolitan area networks—Specific requirements, 2009, http://standards.ieee.org.

[4] IEEE 802.16 Standard for local metropolitan area networks, 2009, http://standards.ieee.org.

[5] Third Generation Partnership Project, http://www.3gpp.org.

[6] Digital video Broadcasting Standards, http://www.dvb.org.

[7] S. R. Saunders, A. A. Aragón -Zavala, “Antennas and Propagation for Wireless Communications”, Second Edition, 2007, *Wiley*, UK.

[8] M. Sellathurai, P. Guinand, and J. Lodge, "Space-Time Coding in Mobile Satellite Communications Using Dual-Polarized Channels", *IEEE Trans. Veh. Tech.*, vol. 55, no 2, January 2006.

[9] K. P. Liolis, J. Gomez-Vilardebo, E. Casini, A. Perez-Neira, “On the Statistical Modelling of MIMO Land Mobile Satellite Channels: A Consolidated Approach”, *IET and AIAA International Communications Satellite Systems Conference*, pp422, Edinburgh, 2009.

[10] F. P. Fontan, P. M. Espiñeira, “Modelling the Wireless Propagation Channel: A simulation approach with MATLAB”, 2008, *Wiley*, UK.

[11] R. G. Vaughan, J. B. Andersen, “Channels, Propagation and Antennas for Mobile Communications”, 2002, *IEE Press*, UK.

[12] M. Gudmundson, ”Correlation model for shadow fading in mobile radio systems”, *IEE Electronics Letters*, vol.27, no.23, 1991, pp.2145-2146.

[13] M. J. Marsan, G. C. Hess and S. S. Gilbert, ”Shadowing variability in an urban land mobile environment at 900MHz”, *IEE Electronics Letters*, vol.26, no.10, 1990, pp.646-648.

[14] M. Pätzold , “Mobile Fading Channels”, *Wiley*, UK, 2002.

[15] J.P. Kermoal, L. Schumacher, K. I. Pedersen, P.E. Mogensen, F. Frederiksen, ”A Stochastic MIMO Radio Channel Model With Experimental Validation”, *IEEE Journal on Selected Areas in Communications*, vol. 20, no. 6, pp1211-1226 August 2002.

**Peter R. King** received the BSc degree in Electronic Engineering (Telecommunications) from the University of Essex, U.K. in 1989, the MSc degree in Mobile & Satellite Communications and the PhD degree in mobile satellite radio propagation from the University of Surrey, U.K. in 2002 and 2007 respectively. He has worked in radio frequency and radio propagation research & development since 1990 for many leading organizations such as Lucent Technologies, Nortel, Roke Manor Research, Samsung, TTP Communications, Airspan, Thales, ITT Defence and AceAxis. He now runs a small RF consultancy business, providing solutions for mobile, satellite, aircraft and wireless radio communication systems, circuits and products. In addition to his consultancy work, he continues to research and teach at the University of Surrey where he is a visiting academic. His research interests include terrestrial and satellite radio propagation, and high-performance radio: power amplifiers, receivers, transmitters, frequency synthesis and power amplifier linearization.

**Tim W. C. Brown** (StudM'00-M'04) graduated from the University of Surrey in 1999 with a BEng in Electronic Engineering and since graduated with a PhD in antenna diversity for mobile terminals in the Centre for Communication Systems Research (CCSR) in 2004. Since completing his doctoral research, he has continued his research interests in antennas, propagation and radio frequency (RF) engineering. This has included postdoctoral research from 2004-2006 at Aalborg University, Denmark and his present post as a lecturer in RF, antennas and propagation at CCSR. His current research interests include mobile terminal antennas, satellite communications, multiple input multiple output (MIMO), ultra wideband (UWB), radar, radio frequency identification (RFID), near field communications (NFC) and vehicular technologies.

**Argyrios Kyrgiazos** received the Dipl.–Eng degree in electrical and computer engineering from the National Technical University of Athens (NTUA) Greece, and the MSc degree in mobile and satellite communications from the University of Surrey UK, in 2008 and 2010 respectively. In 2008, he joined the Greek army for his mandatory duty. He is currently working towards his PhD degree in University of Surrey. His research interests include wireless terrestrial and satellite communications with emphasis on physical layer and link layer issues, and satellite radio propagation. Mr Kyrgiazos is a member of the Institution of Engineering and Technology (IET) and a member of the Technical Chamber of Greece (TEE).

**Barry G. Evans** (M'86–SM'98) Until 2009 was Pro Vice Chancellor for Research and Enterprise at the University of Surrey and Director of the Centre for Communication Systems Research which is a 150 strong postgraduate research centre. Barry has a personal research background in satellite and mobile communications, researching in speech coding, radio propagation, advanced physical layers and cognitive radio with over 500 research publications and three text books to his name. He now runs a number of research projects in satellite communications with ESA and industry and leads the Surrey part of the UK-India network of excellence in next generation networks. He also leads the communications platform in Surrey's Knowledge Transfer Network. He is Editor of the International Journal of Satellite Communications, an OFCOM spectrum advisory board member, chair of the steering committee of SatNEx, an EU/ESA network of excellence, a member of the steering council of the Integral Satellite Initiative and Director of a spin off company Mulsys Ltd. He is a Fellow of the Royal Academy of Engineering.